Divergent trends of open-surface water body area in the contiguous United States from 1984 to 2016

Zhenhua Zou[a], Xiangming Xiao[a,b,1], Jinwei Dong[c], Yuanwei Qin[a], Russell B. Doughty[a], Michael A. Menarguez[d], Geli Zhang[a], and Jie Wang[a]

[a]Department of Microbiology and Plant Biology, Center for Spatial Analysis, University of Oklahoma, Norman, OK 73019; [b]Ministry of Education Key Laboratory of Biodiversity Science and Ecological Engineering, Institute of Biodiversity Science, Fudan University, 200433 Shanghai, China; [c]Key Laboratory of Land Surface Pattern and Simulation, Institute of Geographic Sciences and Natural Resources Research, Chinese Academy of Sciences, 100101 Beijing, China; and [d]LinkedIn Corporation, Sunnyvale, CA 94085

Edited by B. L. Turner, Arizona State University, Tempe, AZ, and approved March 1, 2018 (received for review November 4, 2017)

The contiguous United States (CONUS), especially the West, faces challenges of increasing water stress and uncertain impacts of climate change. The historical information of surface water body distribution, variation, and multidecadal trends documented in remote-sensing images can aid in water-resource planning and management, yet is not well explored. Here, we detected open-surface water bodies in all Landsat 5, 7, and 8 images (~370,000 images, >200 TB) of the CONUS and generated 30-meter annual water body frequency maps for 1984–2016. We analyzed the interannual variations and trends of year-long water body area, examined the impacts of climatic and anthropogenic drivers on water body area dynamics, and explored the relationships between water body area and land water storage (LWS). Generally, the western half of the United States is prone to water stress, with small water body area and large interannual variability. During 1984–2016, water-poor regions of the Southwest and Northwest had decreasing trends in water body area, while water-rich regions of the Southeast and far north Great Plains had increasing trends. These divergent trends, mainly driven by climate, enlarged water-resource gaps and are likely to continue according to climate projections. Water body area change is a good indicator of LWS dynamics in 58% of the CONUS. Following the 2012 prolonged drought, LWS in California and the southern Great Plains had a larger decrease than surface water body area, likely caused by massive groundwater withdrawals. Our findings provide valuable information for surface water-resource planning and management across the CONUS.

water-body area | variation | trend | drought | climate change

Terrestrial open-surface water bodies, including lakes, reservoirs, rivers, streams, and ponds, are critically important water resources for agriculture, aquiculture, industrial production, and aquatic and terrestrial ecosystems (1, 2). Numerous open-surface water bodies are distributed across the contiguous United States (CONUS), providing 99%, 57%, and 63% of the water used in thermoelectric-power production, agricultural irrigation, and public water supply, respectively (3). According to the Water Supply Stress Index model, surface water stress was found in over 9% of the 2,103 CONUS watersheds, mostly distributed in the western half of the United States (4). Climate-change models predicted a general increase of water stress across the United States, with the largest increases in the southwestern United States through 2050 (5). Southwestern states experienced a spate of dryness in the early 21st century (6) and are projected to become drier and experience more severe droughts in the latter half of the 21st century by various climate and hydrology models (7–9). Water-resource managers in the western United States face the challenges of adapting to unprecedented droughts and uncertain impacts of climate change (10). The spatial distribution, temporal dynamics, and long-term trends of CONUS surface water bodies, documented in remote-sensing images in the last three decades, can provide valuable information for water-resource managers in water-resource planning and management in coping with drought and climate change, yet the information has not been well explored.

Strong interannual variability of surface water bodies caused by severe drought events have substantially impacted United States socioeconomic systems (11, 12). In July 2012, United States nuclear-power production hit its lowest seasonal levels in 9 y because of a water shortage and high water temperature (13). The lack of timely rainfall and the scarcity of irrigation water in 2012 caused widespread crop failure across the Great Plains and the midwestern United States (14). Corn and soybean yields in 2012 were 26% and 10%, respectively, below the yields forecasted by the US Department of Agriculture at the beginning of the crop growing season (15). Many reservoirs in the arid and semiarid western regions were depleted during the 2012 drought (15), and contingency plans were activated to maintain public water supply (16). Reduced water body area due to severe droughts also dramatically impacted ecosystems (17, 18). For example, decreased pond water in the southeastern United States led to the rapid decline of salamander occupancy from 22.3% in the spring of 2009 to 9.9% in the fall of 2012 (18). The drought-induced reduction of stream flow and water coverage of the Kiamichi River in southeastern Oklahoma had substantially reduced the freshwater mussel abundance by over 60% from 1992 to 2011 (19). Although the consequences of strong water body variations are evident, the interannual variability and trends

Significance

Strong variations in open-surface water body areas have impacted United States agriculture, economy, society, and ecosystems. This study presents the uneven water-resource distribution across the contiguous United States with the western half of the United States having less water body area but stronger interannual variability compared with the eastern half. Divergent trends of open-surface water body area in the last three decades, mainly driven by climate, indicated that the water-poor regions of the Southwest and Northwest United States were getting poorer, while the water-rich regions of Southeast and far north Great Plains were getting richer. Surface water body shrinkage in drought years led to massive groundwater mining and the rapid decrease of land water storage in California and the southern Great Plains.

Author contributions: Z.Z. and X.X. designed research; Z.Z. and X.X. performed research; Z.Z., X.X., J.D., Y.Q., R.B.D., M.A.M., G.Z., and J.W. analyzed data; and Z.Z., X.X., J.D., Y.Q., R.B.D., M.A.M., G.Z., and J.W. wrote the paper.

The authors declare no conflict of interest.

This article is a PNAS Direct Submission.

Data deposition: The data reported in this work have been deposited in Zenodo (https://doi.org/10.5281/zenodo.1194516).

[1]To whom correspondence should be addressed. Email: xiangming.xiao@ou.edu.

This article contains supporting information online at www.pnas.org/lookup/suppl/doi:10.1073/pnas.1719275115/-/DCSupplemental.

Published online March 26, 2018.

of open-surface water body area across the CONUS in the last three decades have remained unknown.

The spatial distribution and temporal variation of open-surface water bodies are affected by both climate and anthropogenic activities (2, 20). Precipitation and temperature are two dominant climatic factors that affect the changes of open-surface water body area (21, 22). Various anthropogenic activities were also found related to the change of open-surface water bodies, including dam construction (20), water withdrawals for public water supply (23), agricultural irrigation (21), thermoelectric power production (24), and coal, oil, and gas mining (21, 25). Climate change and enhanced demand for public water supply, irrigation, and industrial production in the last three decades have affected United States water resources (2, 9); however, how the climate and human development have affected the variability of surface water body area in individual states across the CONUS have not been examined.

The objective of this study was to fill the above-mentioned knowledge gaps by investigating the interannual variations and trends of surface water body area and how it is affected by climate and anthropogenic factors across the CONUS during 1984–2016. First, we used all available Landsat image archives (~370,000 images, >200 terabytes of data) and a spectral index- and pixel-based approach (23) to detect water bodies and generate annual frequency maps of surface water bodies of the entire CONUS. Second, using these annual frequency maps, we generated annual maps of year-long, seasonal, and ephemeral water bodies. Third, we analyzed the interannual variability of year-long water body area for each state by calculating their SDs, and analyzed their multidecadal trends through linear regressions. Fourth, multiple stepwise regression models were used to assess four primary factors that affect the interannual variability of water body area: precipitation, temperature, surface water withdrawal, and the water body area in the previous year. Fifth, the relationships between open-surface water body area and land water storage (LWS), derived from the gravity recovery and climate experiment (GRACE) liquid water-equivalent thickness (LWET) data (26), were analyzed. Finally, we investigated the impacts of severe drought events on temporal dynamics of surface water body area and LWS in California and the southern Great Plains.

Results and Discussion

Water Body Frequency Maps and Water Body Areas. There were ~428 million 30-m pixels with annual water body frequencies >0 in the CONUS in 2016 (Fig. 1*A*), corresponding to ~385,000-km^2 maximum surface water body area. Water pixels with annual water frequencies ≥0.75 were defined as year-long water bodies, while the other water pixels were classified as seasonal water bodies (≥5%) or ephemeral water bodies (<5%) (23) (*SI Appendix*, *Text S1*). There were about 285 million year-long water pixels (~257,000 km^2) within the CONUS in 2016, comprising the central portions of lakes, reservoirs, and large rivers (Fig. 1*B*), which serve as the major sources for surface water withdrawals. The remaining 143 million seasonal and ephemeral water pixels (~128,000 km^2) are the small streams, ponds, and the edges of large surface water bodies (Fig. 1*B*). The 33-y frequency map of surface water body over 1984–2016 had very similar spatial patterns to the annual water body frequency map of 2016 (Fig. 1 *B* and *D*). According to the 33-y frequency map (Fig. 1*C*), there were 277 million pixels with water frequencies ≥0.75, corresponding to ~250,000 km^2, which is close to the year-long surface water body area in 2016.

Using different frequency thresholds can yield different estimates of surface water body areas (Fig. 1*E*), such as the year-long (≥0.75), seasonal (0.05–0.75), and ephemeral (<0.05) water body areas during 1984–2016. At the CONUS scale, the year-long water body area varied from 246,641 km^2 to 261,328 km^2 in the last three decades, with small variability according to its SD (2,977 km^2). Year-long water body areas at the CONUS scale have no significant trends during 1984–2016. However, significant increasing trends were found in both seasonal (R^2 = 0.34, P < 0.001) and ephemeral (R^2 = 0.59, P < 0.001) water body areas, which might be related to the increase of large rainfall events and rainfall intensity in the CONUS (9, 27).

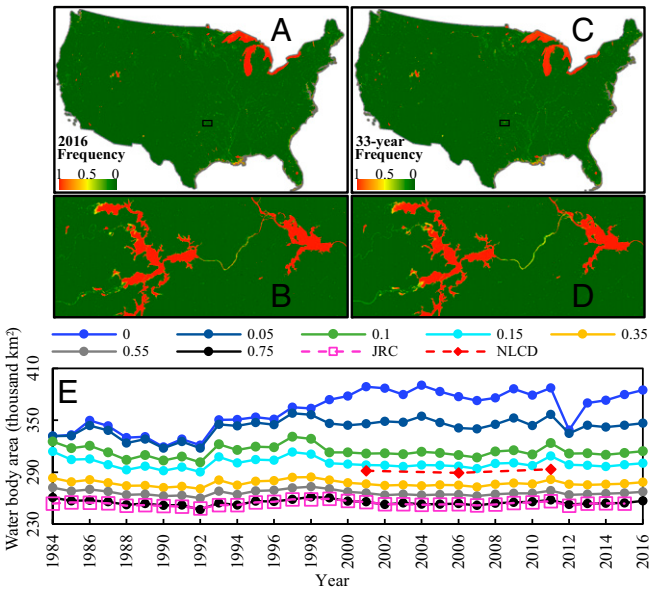

Fig. 1. Water body frequency maps and water body areas using different frequency thresholds in the CONUS. (*A*) Annual water body frequency map in 2016 and (*B*) its zoom-in view of eastern Oklahoma. (*C*) A 33-y water body frequency map during 1984–2016 and (*D*) its zoom-in view of eastern Oklahoma. (*E*) Total water body area of all pixels within CONUS with water body frequencies >0, ≥0.05, ≥0.1, ≥0.15, ≥0.35, ≥0.55, and ≥0.75, respectively, in our datasets; the permanent water body areas from the JRC dataset during 1984–2015; and the water body area from NLCD in 2001, 2006, and 2011. Water body frequency is the ratio of water body observations to total good observations in a year (*A*) or all 33 y during 1984–2016 (*C*).

We compared the year-long water body areas in the CONUS from our dataset with those from the Joint Research Centre (JRC) (20) and National Land Cover Database (NLCD) (28) (Fig. 1*E*). The total area and interannual variability of year-long water bodies from our dataset agreed well with those from the JRC permanent water bodies (Fig. 1*E*), which were derived from analysis of all available Landsat top-of-atmosphere reflectance images during 1984–2015 (20). It is interesting to note that total CONUS water body areas from the NLCD in 2001, 2006, and 2011 (28) were much higher than our year-long water body area and the JRC permanent water body area (Fig. 1*E*). The water body areas of the NLCD could include some seasonal or ephemeral water bodies, as the NLCD project used only a few good quality Landsat images taken during the plant growing season (28), which is often the wet season when more of the land surface is inundated with water. The good agreement between the year-long water body area from our dataset and the permanent water body area from the JRC dataset clearly demonstrates the value of analyzing all available Landsat images in the study of land and water dynamics.

Water Body Distribution, Variation, and Driving Factors. Surface water bodies are distributed unevenly across the CONUS with various interannual variabilities (Fig. 2*A*). The average water body area (hectare, ha) per unit land (square kilometer) during 1984–2016 ranged from 0.2 ha/km^2 in Arizona and New Mexico to 40.7 ha/km^2 in Michigan, while its SD ranged from 0.0001 ha/km^2 in Washington, DC to 0.8 ha/km^2 in Utah. Most of the western half of the United States have surface water body areas <1 ha/km^2. Water resources in these regions have strong interannual variability based on the various SDs of water body area during 1984–2016 (Fig. 2*A*). The western, especially southwestern United

SUSTAINABILITY SCIENCE

States, was identified as a hotspot for water shortages in various hydrological model assessments and projections (4, 29, 30). Water shortages in these areas were aggravated by large water withdrawals for agriculture (31) and thermal-electric power plants (9). Because of the limited water resources, many regions in the southwestern and northwestern United States have to import water from beyond their watersheds (32). The water body area in the southeastern United States is ∼1 ha/km^2 higher than those of the western half of the United States, and had relatively small interannual variations based on their small SDs (Fig. 2*A*). Despite the abundance in water resources, the southeastern United States remains vulnerable to changes in water supply and demand (9). Utah has a much larger water body area than its neighboring states because of the Great Salt Lake, and the states in the Great Lakes Region have the highest surface water body areas because of the Great Lakes. Overall, the eastern half of the United States has more water body area and less variability than the western half, which is similar to the spatial patterns of annual precipitation (*SI Appendix*, Fig. S1).

The year-long water body areas by individual states during 1984–2016 showed remarkably divergent trends over years (Fig. 2*B*). All eight states in the Southwest and Northwest, plus Oklahoma and Washington, DC, had significant decreasing trends in their year-long water body areas during 1984–2016. According to the slopes of simple linear regression models, the decreasing rates of year-long water body area (square meter) per unit land area (square kilometer) ranged from 18 m^2/km^2 per year in Colorado to 465 m^2/km^2 per year in Utah. In contrast, 20 states in the Southeast, far north Great Plains, and southern Midwest had significant increasing trends in their year-long water body areas during 1984–2016. The increasing rates ranged from 14 m^2/km^2 per year in Iowa to 458 m^2/km^2 per year in North Dakota. The remarkable interannual divergent trends of year-long water body area were also found among the 336 watersheds within the CONUS (Fig. 2*C*). Eighty-one watersheds, mostly in the Southwest and Northwest, had significant decreasing trends, ranging from 3 m^2/km^2 per year in the Rio De Bavispe Watershed of Arizona to 1,355 m^2/km^2 per year in the Carson Watershed of Nevada (Fig. 2*C*). Ninety-seven watersheds, mostly in the Southeast and far north Great Plains, had significant increasing trends, ranging from 3 m^2/km^2 per year in the Mimbres Watershed of New Mexico to 1,799 m^2/km^2 per year in the Central Louisiana Coastal Watershed of Louisiana (Fig. 2*C*). Most of the significant decreasing trends of surface water body area were found in states and watersheds that have relatively small water body areas and large interannual variabilities, while most of the significant increasing trends were found in states and watersheds that have relatively large water body areas and small variabilities. Thus, in general, the water-poor regions of the southwestern and northwestern United States were becoming poorer, while the water-rich regions of the southeastern United States and far north Great Plains were becoming richer over the last three decades.

Climate is the main factor contributing to the interannual variations of surface water body area. Annual precipitation was a significant variable in multiple stepwise regression models for most of states (*SI Appendix*, Fig. S2*C*), demonstrating its influence on water body area decrease in the Northwest and Southwest, and the water body area increase in the Southeast and far north Great Plains. Annual average temperature was a significant variable for the water body area decrease in the Northwest, as well as New Mexico, Oklahoma, and Mississippi (*SI Appendix*, Fig. S2*D*). Surface water withdrawals showed significant influences in only a few states (*SI Appendix*, Fig. S2*E*), which could be caused by the water-withdrawal regulations associated with water availability, and the infrequent water withdrawal data, reported every 5 y (3). Water body area in the previous year had significant positive impact in most multiple stepwise regression models, indicating strong legacy effects, especially in the western half of the United States (*SI Appendix*, Fig. S2*F*). It is also worth noting that about 90% of the ∼8,000 major dams within the CONUS were

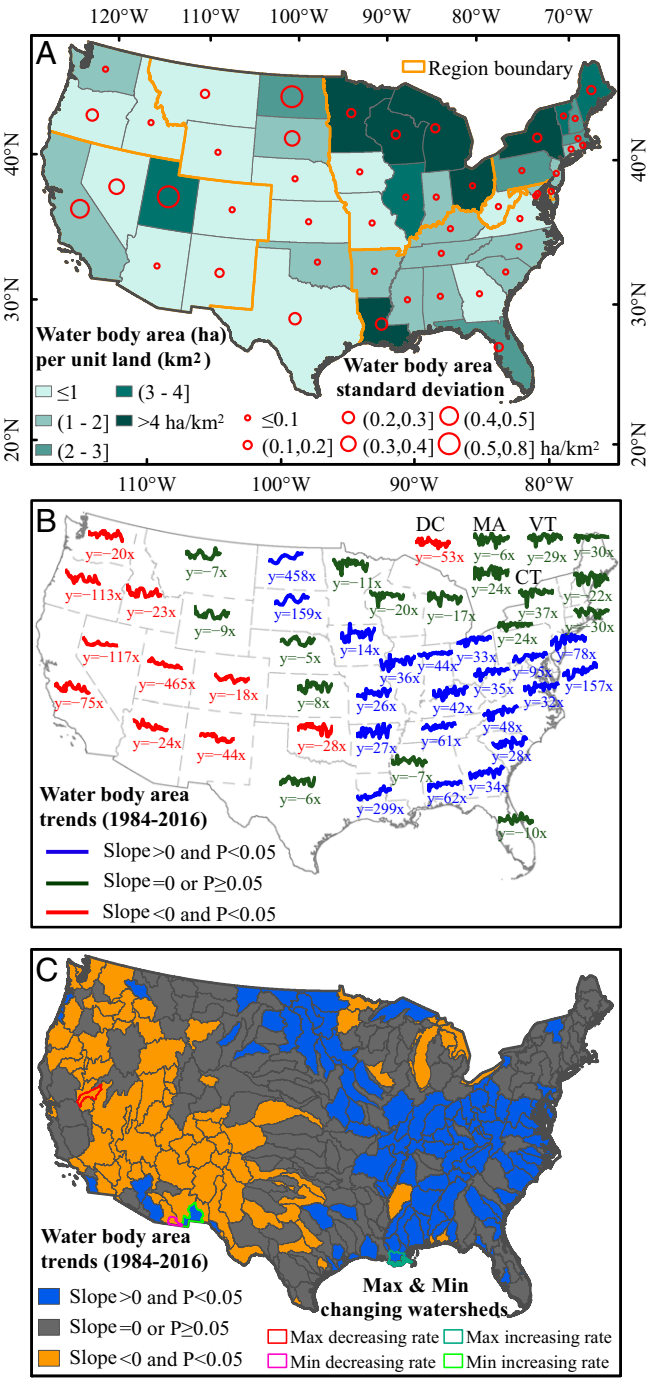

Fig. 2. Year-long water body area and interannual trends in the CONUS during 1984–2016 by states and watersheds. (*A*) Average and SD of year-long water body area (ha) per unit land (km^2) during 1984–2016 by states [the region boundary was based on the Third National Climate Assessment (9)]. The middle region is the Great Plains, while on its left are the Northwest and Southwest, and on its right are the Midwest, Northeast, and Southeast. The western half of the United States in this study consists of the Northwest, Southwest, and the Great Plains, while the eastern half of the United States consists of the Midwest, Northeast, and Southeast). Interannual trends of year-long water body area (m^2) per unit land (km^2) during 1984–2016 with *t* test at the 5% significance level by states (*B*) and by watersheds [six-digit Hydrologic Units Code (HUC-6)] (*C*). The intercepts of simple linear regression models in *B* are not shown because of limited space. Slope is the coefficient of independent variable *x*, which is the year.

constructed before 1984 (33), while the 735 dams constructed during 1984–2003 had an even spatial and temporal distribution (*SI Appendix*, Fig. S3). Thus, the observed divergent trends of open-surface water body area during 1984–2016 were largely driven by climate factors rather than by human water withdrawals or dam construction. The divergent trends are likely to continue in the future given the strong drying forecast in the Southwest and strong wetting forecast in the eastern United States by climate model simulations (34).

Water Body Area and LWS. We investigated spatial-temporal variability of year-long water body area in relation to LWS dynamics as observed by the GRACE satellite in the CONUS. GRACE LWS during 2002–2016 showed that large areas of 10 states in the Southwest, southern Great Plains, and northern Midwest had significant decreasing trends (Fig. 3*A*). In contrast, significant increasing trends of LWS were found in more than 20 states in the Northwest, northern Great Plains, Midwest, and Northeast. The changes of LWS in a grid cell is affected by surface water body, soil moisture, groundwater, and water in vegetation (35). We aggregated the annual maps of year-long water bodies at 30-m resolution into 0.5° (latitude and longitude) grid cells (Fig. 3*B*). The trends of year-long water body area during 2002–2016 were more dispersive, with significant decreasing trends mostly distributed in California and northern Minnesota, and significant increasing trends mostly concentrated in the northern Great Plains and southeastern United States (Fig. 3*B*). The linear regression models between LWS and year-long water body areas during 2002–2016 showed significant positive correlations (slope > 0 and $P < 0.05$) in 58% of the 2,818 0.5° grid cells within the CONUS (Fig. 3 *C* and *D*), mostly in California, the Great Plains, and the Southeast. Open-surface water bodies (lakes, reservoirs, rivers, and ponds) were found to be related to the dynamics of groundwater (36) and total LWS (37). In the water body-abundant Prairie Coteau (38,000 km^2), surface water bodies accounted for a significant fraction of GRACE LWS and improved the water-budget closure estimation (37). The significant positive correlations between surface water body area and LWS suggested that the change in year-long water body area is a strong indicator of LWS dynamics.

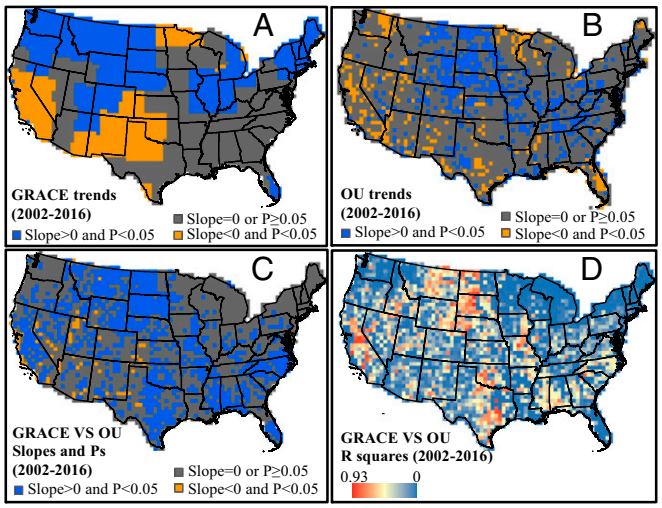

Fig. 3. The slopes, *P* values and r^2 values of simple linear regression models of GRACE LWS and year-long water body area at 0.5° grid cells during 2002–2016 with *t* test at the 5% significance level. (*A*) GRACE LWS over years. (*B*) Year-long water body area from our datasets (OU datasets) over years. (*C* and *D*) GRACE LWS (dependent variable) over OU year-long water body area (independent variable).

The Effects of Drought on Water Body Area and LWS. Severe and prolonged droughts can substantially reduce surface water body area. California and the southern Great Plains are among the top agricultural-producing states, where surface water withdrawals play an important role in crop irrigation and livestock production (3). The interannual variation of year-long water body area in California clearly showed four multiyear dry and pluvial rotation events (Fig. 4*A*), three of which corresponded to documented drought events in 1986–1992, 2007–2009, and 2012–2015 (38). Surface water body areas had substantial drops at the beginning of drought events in 1986, 2007, and 2012, reached their lows at the end of these drought events in 1992, 2009, and 2015, and took several more years for the first two drought events to recover fully in 1995 and 2011. As of 2016, surface water body area had not yet recovered from the most recent drought event. The 2012–2015 drought caused the surface water body areas to drop to their lowest levels in 33 y (Fig. 4*A*). Precipitation in California in 2016 was above the average value of 1984–2016, but resulted in only a minor recovery of surface water body area. In contrast, the southern Great Plains were dominated by 1- to 2-y drought events: for example, the 2006 drought in Kansas, Oklahoma, and Texas (39); the 2011 and 2012 drought in Oklahoma and Texas; and the 2012 drought in Kansas (12). Surface water body areas in Kansas, Oklahoma, and Texas dropped in the dry year of 2006 and recovered quickly in the subsequent pluvial year of 2007 (Fig. 4 *B*–*D*). The southern Great Plains suffered a prolonged drought that developed in 2011 and reached peak intensity in August 2012 (12). The year-long water body areas in these three states dropped during 2011–2012, stayed low through 2014, and recovered gradually to their normal condition in 2016. The southern Great Plains had an extremely pluvial year of 2015 because of El Niño teleconnection (40), which aided the recovery of surface water body area.

Prolonged droughts can result in a larger decline of LWS than surface water body area. In California and the southern Great Plains, the interannual variability of surface water body areas during 2002–2012 agreed well with those of LWS (Fig. 4). However, because of prolonged droughts, LWS had a much larger decline than surface water body areas in California and the southern Great Plains during 2014–2015 and 2013–2014, respectively. The California Central Valley relied heavily on groundwater to mitigate droughts (41). The 2014–2016 droughts reduced surface water availability by 7.6 km^3/y and increased groundwater use by 6.2 km^3/y compared with an average water year (41). The rate of groundwater decline in the California Central Valley predicted by the water-balance models (10.0 km^3/y) that used a large amount of in situ observations was quite close to that inferred from GRACE (11.2 km^3/y) during the 2012–2016 droughts (42). Observation data from 497 wells in the California Central Valley showed that droughts played a major role in the depletion of groundwater through increased well drilling and water extraction (43). The shrinkage of surface water bodies in drought years had forced water users to drill and mine groundwater (38, 44), which could have caused the larger decrease of LWS. Groundwater in the California Central Valley was being pumped at far greater rates (20.4 mm y^{-1}) than it can be naturally replenished, which may raise economic and food-security challenges for the United States (45). The in situ observation data from ∼10,000 High Plains aquifer wells also indicated severe drought-induced groundwater declines in southern and central High Plains aquifers in 2012 (46). Based on the water-level data from 7,460 wells during 2011–2013, the area-weighted, average water level in the High Plains aquifer declined by 0.64 m, with major declines in the south and central High Plains, Texas (1.1 m), Kansas (0.9 m), Colorado (0.7 m), and Oklahoma (0.6 m) (47). Groundwater depletion in the irrigated southern Great Plains and California Central Valley accounted for ∼50% of groundwater depletion of the entire United States since 1900 (48). With the low recharge rate in central and southern High Plains aquifer, the current depletion rate would result in 35% of the southern High Plains lacking sufficient irrigation water in the next

SUSTAINABILITY SCIENCE

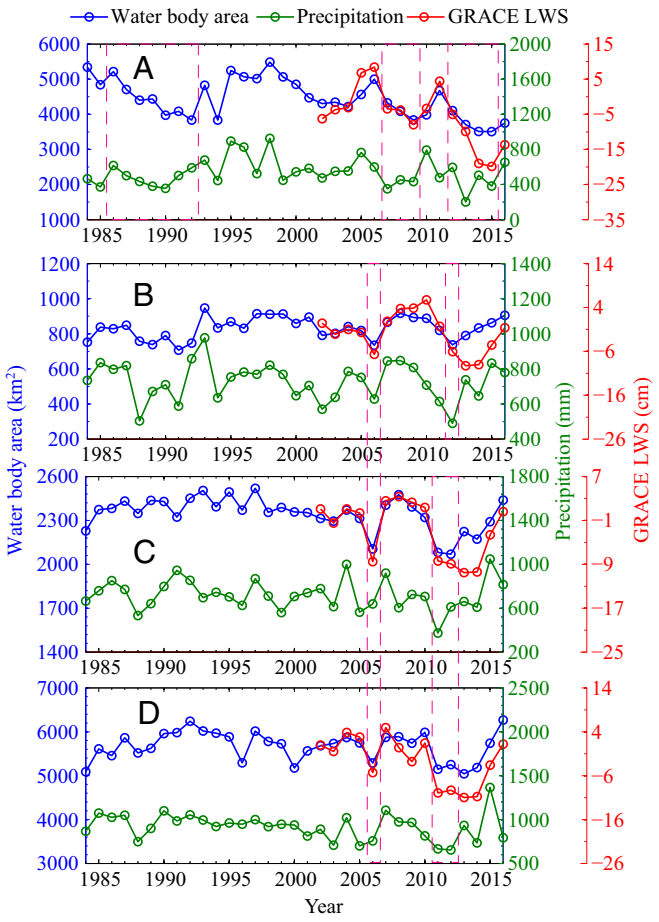

Fig. 4. Interannual variations of year-long water body area, GRACE LWS, and annual precipitation during 1984–2016 in California (*A*), Kansas (*B*), Oklahoma (*C*), and Texas (*D*). The dashed pink box indicates documented drought events, including 1986–1992, 2007–2009, and 2012–2015 droughts in California; 2006 drought in Kansas, Oklahoma, and Texas; 2011–2012 drought in Oklahoma and Texas; and 2012 drought in Kansas.

30 y (48). The depletion of groundwater could in turn decrease the discharge to surface water bodies (22), aggravating surface water scarcity in these regions.

Conclusions and Perspective

Consistent with previous studies (4, 5), the western half of the United States was identified as a hotspot of water stress with small water body area and large interannual variability in this study. Mainly driven by climate, year-long water body areas were shrinking in water-poor regions of the southwestern and northwestern United States but expanding in water-rich regions of the Southeast and far north Great Plains. These divergent changes have enlarged the water resource gaps across the CONUS in the last three decades. Thus, water-resource management is becoming more and more challenging in the western United States, especially during the 2012 prolonged droughts (15). Various climate and hydrological models have predicted the Southwest to be drier and face more severe droughts in the second half of the 21st century (8, 9, 34), aggravating the challenges in water-resource planning and management. The results from the analyses of historical Landsat images during 1984–2016 clearly shed new insight on the spatial distribution, temporal dynamics, and long-term trends of open-surface water bodies in the CONUS and highlight the unoptimistic surface water body conditions in the Southwest and Northwest. These findings can be used to assist decision makers and stakeholders across the CONUS, especially in the West, to develop and implement water-resource planning and management in coping with the increasing water stress, unprecedented droughts, and uncertain impacts of climate change.

Materials and Methods

Landsat Image. This study used all Landsat 5, 7, and 8 surface reflectance images of the entire CONUS (~370,000 images, >200 terabytes of data) in the Google Earth Engine platform (49), which were originally from the US Geological Survey Earth Resources Observation and Science (EROS) Center (50, 51). The number of images used in a year ranges from 3,501 in 1984 to 17,409 in 2014, with more images after the launch of Landsat 7 in 1999 (*SI Appendix*, Fig. S4*A*). For each image, the CFmask band was used as a quality control band to remove the cloud, cloud shadow, and snow pixels. The solar azimuth and zenith angles of each image were used along with the Shuttle Radar Topography Mission digital elevation model (52) to simulate terrain shadows and remove them. The remaining pixels were considered as good observations that can be used for water body detection. The pixels with zero good observations in a year account for 0.27% on average during 1984–1998 and 0.04% during 1999–2016 (*SI Appendix*, Fig. S4*B*). More than 99.95% of the pixels within the CONUS had a total number of good observations ≥33 in the last 33 y, while the majority of the pixels have a total number of good observations ranging from 300 to 1,200 (*SI Appendix*, Fig. S4*C*).

Data on LWS, Water Withdrawal, and Climate. The GRACE monthly LWET products during 2002–2016 were the anomalies relative to the 2004.0–2009.999 time-mean baseline (26). The mascon-set of 0.5° gain factors were applied to the LWET data over land before further analysis. Monthly LWET data were used to calculate annual average LWET data, which were then used as the LWS values to explore its relationships with surface water body area. State-level water withdrawals, gathered every 5 y by the US Geological Survey (3), were interpolated into annual water withdrawal data (*SI Appendix*, *Text S2*) and used as a predictor variable in the multiple stepwise regression models for interannual variations of water body area. Statewide annual precipitation and annual average temperature data were gathered from the National Centers for Environmental Information (53) and also used as predictor variables.

Water Body Detection and Verification. The relationship between water and vegetation indices can be used to detect open-surface water bodies (54, 55), and the water body mapping algorithm with analysis of time series Landsat images was reported in a study for Oklahoma (23). Systematic and random sampling methods were used to select 32 sampling plots across the CONUS (*SI Appendix*, Fig. S5), which together had a total of 1.26 million water and nonwater pixels. The modified Normalized Difference Water Index (mNDWI), Enhanced Vegitation Index (EVI), and Normalized Difference Vegitation Index (NDVI) (*SI Appendix*, *Text S3*) of each pixel in the 32 plots were calculated. According to the spectral index distribution of ~1.26 million water and nonwater sampling pixels across the United States (*SI Appendix*, Fig. S6), we classified the pixels whose water signal was stronger than the vegetation signal as open-surface water bodies using criteria mNDWI > EVI or mNDWI >NDVI (*SI Appendix*, *Text S4*). To further remove the vegetation noise, EVI < 0.1 was used to remove the mixed pixels of water and vegetation. Therefore, only the pixels that met the criteria [(mNDWI > NDVI or mNDWI > EVI) and (EVI < 0.1)] were classified as open-surface water body pixels while the rest were classified as nonwater pixels. The algorithms were verified using ~12,000 randomly sampled Landsat pixels across the CONUS (*SI Appendix*, *Text S5* and Figs. S7 and S8) and showed an overall accuracy of 96.91% with a κ coefficient of 0.94 for pure water and nonwater pixels (*SI Appendix*, *Text S5* and Table S1).

The water detection algorithms were performed on every good observation pixel in the ~370,000 Landsat images in the platform of Google Earth Engine, a cloud-based geospatial processing platform with large storage and processing power (https://developers.google.com/earth-engine/). For each pixel, its annual and 33-y water body frequency was defined as the ratio of water observations to total good observations (water and nonwater observations) in a year and in 1984–2016, respectively. The 33-y water body frequency map was used to generate a nonwater mask (33-y water body frequency <0.01) and a permanent water mask (33-y water body frequency ≥0.95), which were then applied to the annual water frequency maps to remove low-frequency noise caused by residual cloud, cloud shadow, and to fill the no data values. In each year, the annual water body frequency of pixels masked by the nonwater mask and permanent water mask were set to 0 and 1, respectively.

Statistical Analyses. Based on annual water body frequency maps, year-long water body areas were calculated for each of the last 33 y. The interannual variability and trends of water body area during 1984–2016 by individual states and watersheds were calculated and analyzed through linear regression models with *t* test at the 5% significance level. The year-long water body areas within 0.5° grid cells were summed in each year of 2002–2016, and their linear relationships with LWS were examined in each of the 2,818 0.5° grid cells across the CONUS. Multiple stepwise linear regressions were carried out in the platform of MATLAB R2014a to analyze the relationships between statewide year-long water body areas and four predictor variables, including annual precipitation, annual average temperature, annual surface water withdrawal, and the year-long water body area of the previous year. Water body area of the previous year was included as a predictor variable because of the legacy effect. No strong collinearity among the predictor variables was found (*SI Appendix*, Table S2).

ACKNOWLEDGMENTS. We thank Sarah L. Xiao at the University of Oklahoma for English language editing, and two reviewers for their constructive comments and suggestions for the earlier version of the manuscript. This study was supported in part by research grants from the National Institute of Food and Agriculture, US Department of Agriculture (2013-69002), the National Science Foundation Established Program to Stimulate Competitive Research program (OIA-1301789), and the Department of the Interior, United States Geological Survey to AmericaView (G14AP00002).

1. Wood EF, et al. (2011) Hyperresolution global land surface modeling: Meeting a grand challenge for monitoring Earth's terrestrial water. *Water Resour Res* 47:1–10.
2. Bates BC, Kundzewicz ZW, Wu S, Palutikof JP (2008) *Climate Change and Water. Technical Paper of the Intergovernmental Panel on Climate Change* (IPCC Secretariat, Geneva).
3. US Geological Survey (2010) *Estimated Use of Water in the United States in 1985, 1990, 1995, 2000, 2005 and 2010* (USGS, Reston, VA).
4. Averyt K, et al. (2013) Sectoral contributions to surface water stress in the coterminous United States. *Environ Res Lett* 8:035046.
5. Blanc E, et al. (2014) Modeling US water resources under climate change. *Earths Future* 2:197–224.
6. MacDonald GM, et al. (2008) Climate warming and 21st-century drought in Southwestern North America. *Eos (Washington DC)* 89:82.
7. Cayan DR, et al. (2010) Future dryness in the southwest US and the hydrology of the early 21st century drought. *Proc Natl Acad Sci USA* 107:21271–21276.
8. Scheff J, Frierson DMW (2012) Robust future precipitation declines in CMIP5 largely reflect the poleward expansion of model subtropical dry zones. *Geophys Res Lett* 39: L18704.
9. Melillo JM, Richmond T, Yohe G (2014) *Climate Change Impacts in the United States: Third National Climate Assessment* (US Global Change Research Program, Washington, DC).
10. Miller WP, Piechota TC (2011) Trends in western US snowpack and related Upper Colorado river basin streamflow. *J Am Water Resour Assoc* 47:1197–1210.
11. Hall JW, et al. (2014) Water security. Coping with the curse of freshwater variability. *Science* 346:429–430.
12. Hoerling M, et al. (2014) Causes and predictability of the 2012 Great Plains drought. *Bull Am Meteorol Soc* 95:269–282.
13. Argonne National Laboratory (2012) *Impacts of Long-Term Drought on Power Systems in the U.S. Southwest, Prepared for the U.S. Department of Energy* (US Department of Energy, Washington, DC).
14. Wolf S, et al. (2016) Warm spring reduced carbon cycle impact of the 2012 US summer drought. *Proc Natl Acad Sci USA* 113:5880–5885.
15. Hoerling M, et al. (2013) *An Interpretation of the Origins of the 2012 Central Great Plains Drought* (NOAA Drought Task Force Narrative Team, Silver Spring, MD).
16. Murti M, et al. (2016) Impact of the 2012 extreme drought conditions on private well owners in the United States, a qualitative analysis. *BMC Public Health* 16:430.
17. Atkinson CL, Julian JP, Vaughn CC (2014) Species and function lost: Role of drought in structuring stream communities. *Biol Conserv* 176:30–38.
18. Walls SC, Barichivich WJ, Brown ME, Scott DE, Hossack BR (2013) Influence of drought on salamander occupancy of isolated wetlands on the southeastern coastal plain of the United States. *Wetlands* 33:345–354.
19. Vaughn CC, Atkinson CL, Julian JP (2015) Drought-induced changes in flow regimes lead to long-term losses in mussel-provided ecosystem services. *Ecol Evol* 5:1291–1305.
20. Pekel JF, Cottam A, Gorelick N, Belward AS (2016) High-resolution mapping of global surface water and its long-term changes. *Nature* 540:418–422.
21. Tao S, et al. (2015) Rapid loss of lakes on the Mongolian Plateau. *Proc Natl Acad Sci USA* 112:2281–2286.
22. Krueger ES, Yimam YT, Ochsner TE (2017) Human factors were dominant drivers of record low streamflow to a surface water irrigation district in the US southern Great Plains. *Agric Water Manage* 185:93–104.
23. Zou Z, et al. (2017) Continued decrease of open surface water body area in Oklahoma during 1984-2015. *Sci Total Environ* 595:451–460.
24. van Vliet MTH, et al. (2012) Vulnerability of US and European electricity supply to climate change. *Nat Clim Change* 2:676–681.
25. Murray KE (2013) State-scale perspective on water use and production associated with oil and gas operations, Oklahoma, U.S. *Environ Sci Technol* 47:4918–4925.
26. Wiese DN (2015) GRACE Monthly Global Water Mass Grids NETCDF RELEASE 5.0 (Jet Propulsion Laboratory, Pasadena, CA), Version 5.0.PO.DAAC.
27. Feng Z, et al. (2016) More frequent intense and long-lived storms dominate the springtime trend in central US rainfall. *Nat Commun* 7:13429.
28. Homer C, et al. (2015) Completion of the 2011 National Land Cover Database for the conterminous United States–Representing a decade of land cover change information. *Photogramm Eng Remote Sens* 81:345–354.
29. Gaupp F, Hall J, Dadson S (2015) The role of storage capacity in coping with intra- and inter-annual water variability in large river basins. *Environ Res Lett* 10:125001.
30. Strzepek K, Boehlert B (2010) Competition for water for the food system. *Philos Trans R Soc Lond B Biol Sci* 365:2927–2940.
31. Caldwell PV, Sun G, McNulty SG, Cohen EC, Myers JAM (2012) Impacts of impervious cover, water withdrawals, and climate change on river flows in the conterminous US. *Hydrol Earth Syst Sci* 16:2839–2857.
32. Good SP, et al. (2014) Patterns of local and nonlocal water resource use across the western US determined via stable isotope intercomparisons. *Water Resour Res* 50: 8034–8049.
33. National Atlas of the United States (2006) *Major Dams of the United States* (National Atlas of the United States, Reston, VA).
34. Strzepek K, et al. (2015) Benefits of greenhouse gas mitigation on the supply, management, and use of water resources in the United States. *Clim Change* 131:127–141.
35. Famiglietti JS (2004) Remote sensing of terrestrial water storage, soil moisture and surface waters. *The State of the Planet: Frontiers and Challenges in Geophysics*, eds Sparks RSJ, Hawkesworth CJ (American Geophysical Union, Washington, DC), Vol 150, pp 197–207.
36. Brunner P, Cook PG, Simmons CT (2009) Hydrogeologic controls on disconnection between surface water and groundwater. *Water Resour Res* 45:W01422.
37. Proulx RA, Knudson MD, Kirilenko A, VanLooy JA, Zhang XD (2013) Significance of surface water in the terrestrial water budget: A case study in the Prairie Coteau using GRACE, GLDAS, Landsat, and groundwater well data. *Water Resour Res* 49: 5756–5764.
38. California Department of Water Resources (2015) *California's Most Significant Droughts: Comparing Historical and Recent Conditions* (Calif Dep Water Resour, Sacramento, CA).
39. Dong X, et al. (2011) Investigation of the 2006 drought and 2007 flood extremes at the southern Great Plains through an integrative analysis of observations. *J Geophys Res* 116:D03204.
40. Wang SYS, Huang WR, Hsu HH, Gillies RR (2015) Role of the strengthened El Nino teleconnection in the May 2015 floods over the southern Great Plains. *Geophys Res Lett* 42:8140–8146.
41. Howitt R, Medellín-Azuara J, MacEwan D, Lund JR, Sumner D (2014) *Economic Analysis of the 2014 Drought for California Agriculture* (Center for Watershed Sciences Univ of California, Davis, CA).
42. Xiao M, et al. (2017) How much groundwater did California's Central Valley lose during the 2012-2016 drought? *Geophys Res Lett* 44:4872–4879.
43. Wang SYS, Lin YH, Gillies RR, Hakala K (2016) Indications for protracted groundwater depletion after drought over the Central Valley of California. *J Hydrometeorol* 17: 947–955.
44. Thomas BF, et al. (2017) GRACE Groundwater Drought Index: Evaluation of California Central Valley groundwater drought. *Remote Sens Environ* 198:384–392.
45. Famiglietti JS (2014) The global groundwater crisis. *Nat Clim Change* 4:945–948.
46. Brena-Naranjo JA, Kendall AD, Hyndman DW (2014) Improved methods for satellite-based groundwater storage estimates: A decade of monitoring the high plains aquifer from space and ground observations. *Geophys Res Lett* 41:6167–6173.
47. McGuire VL (2014) Water-level changes and change in water in storage in the High Plains aquifer, predevelopment to 2013 and 2011-13 (Department of the Interior, US Geological Survey, Washington, DC), US Geological Survey Scientific Investigations Report 2014-5218.
48. Scanlon BR, et al. (2012) Groundwater depletion and sustainability of irrigation in the US High Plains and Central Valley. *Proc Natl Acad Sci USA* 109:9320–9325.
49. Google Earth Engine (2017) *USGS Landsat 5/7/8 Surface Reflectance (Pre-Collection)* (Google Earth Engine, Mountain View, CA).
50. USGS (2017) Landsat 8 Surface Reflectance Code (LaSRC) Product Guide (Department of the Interior US Geological Survey, Washington, DC), Version 3.4.
51. USGS (2017) Landsat 4-7 Climate Data Record (CDR) Surface Reflectance Product Guide (Department of the Interior US Geological Survey, Washington, DC), Version 7.2.
52. Farr TG, et al. (2007) The shuttle radar topography mission. *Rev Geophys* 45:1–33.
53. NOAA (2017) *Climate at a Glance: US Time Series* (National Centers for Environmental Information, Asheville, NC).
54. Dong JW, et al. (2015) Tracking the dynamics of paddy rice planting area in 1986-2010 through time series Landsat images and phenology-based algorithms. *Remote Sens Environ* 160:99–113.
55. Xiao XM, et al. (2006) Mapping paddy rice agriculture in South and Southeast Asia using multi-temporal MODIS images. *Remote Sens Environ* 100:95–113.